

living cells and strongly support our model of ligand-induced reorganization of the EPOR dimer (27). EPOR, and perhaps other cytokine receptors (28), would then exist as unliganded dimers on the cell surface. The hormone would trigger a switch between a self-associated, inactive conformation and an active, ligand-bound conformation. Agonists and antagonists would then have to consider self association as a competing reaction, but small-molecule antagonists for this family of receptors could now be designed to stabilize the inactive dimeric form. Finally, plasticity of receptor binding sites in ligand recognition is emerging as a prevalent theme throughout biology (21, 29). The structure of the human growth hormone receptor initially showed that the same receptor binding site residues interact with completely different faces of its hormone ligand (16). In the EPOR system, the same binding site interacts with two sites on EPO (13), various EMPs (11, 12), and now with itself.

References and Notes

1. S. B. Krantz, *Blood* **77**, 419 (1991); K. Jacobs *et al.*, *Nature* **313**, 806 (1985).
2. J. A. Wells and A. M. de Vos, *Annu. Rev. Biochem.* **65**, 609 (1996); J. F. Bazan, *Proc. Natl. Acad. Sci. U.S.A.* **87**, 6934 (1990).
3. M. Murakami *et al.*, *Proc. Natl. Acad. Sci. U.S.A.* **88**, 11349 (1991); N. Jiang, T. C. He, A. Miyajima, D. M. Wojchowski, *J. Biol. Chem.* **271**, 16472 (1996).
4. O. Miura and J. N. Ihle, *Arch. Biochem. Biophys.* **306**, 200 (1993); D. L. Barber, J. C. DeMartino, M. O. Showers, A. D'Andrea, *Mol. Cell. Biol.* **14**, 2257 (1994); D. J. Matthews, R. S. Topping, R. T. Cass, L. B. Giebel, *Proc. Natl. Acad. Sci. U.S.A.* **93**, 9471 (1996).
5. S. S. Watowich *et al.*, *Proc. Natl. Acad. Sci. U.S.A.* **89**, 2140 (1992); S. S. Watowich, D. J. Hilton, H. F. Lodish, *Mol. Cell. Biol.* **14**, 3535 (1994).
6. J. S. Philo, K. H. Aoki, T. Arakawa, L. Owens-Narhi, J. Wan, *Biochemistry* **35**, 1681 (1996).
7. B. A. Witthuhn *et al.*, *Cell* **74**, 227 (1993); O. Miura *et al.*, *Blood* **84**, 1501 (1994).
8. S. Elliott, T. Lorenzini, D. Yanagihara, D. Chang, G. Elliott, *J. Biol. Chem.* **271**, 24691 (1996); H. Schneider *et al.*, *Blood* **89**, 473 (1997).
9. N. C. Wrighton *et al.*, *Science* **273**, 458 (1996).
10. D. L. Johnson *et al.*, *Biochemistry* **37**, 3699 (1998).
11. O. Livnah *et al.*, *Science* **273**, 464 (1996).
12. O. Livnah *et al.*, *Nature Struct. Biol.* **5**, 993 (1998).
13. R. S. Syed *et al.*, *Nature* **395**, 511 (1998).
14. D. L. Johnson *et al.*, *Protein Expr. Purif.* **7**, 104 (1996).
15. The two independent EBP monomers of the dimer have a root mean square deviation (rmsd) of 0.52 Å for all C α .
16. A. M. de Vos, M. Ultsch, A. A. Kosiakoff, *Science* **255**, 306 (1992); M. Sundstrom *et al.*, *J. Biol. Chem.* **271**, 32197 (1996); W. Somers *et al.*, *Nature* **372**, 478 (1994); M. R. Walter *et al.*, *ibid.* **376**, 230 (1995).
17. M. L. Connolly, *J. Appl. Crystallogr.* **16**, 548 (1983); *ibid.* p. 439. The buried surface calculations were carried out by the program MS with a probe radius of 1.7 Å.
18. The L2 loop is a common component of the binding determinants in the cytokine receptor superfamily (13, 16) but is located in the most distal part of the receptor NH₂-terminal D1 domain between strands C and C'. Thus, in the crystal structures of EBP with the smaller EMP peptide ligands (17) and the native EBP, L2 does not participate in ligand binding.
19. Hydrogen bonds are made, for example, between His¹⁵³ imidazole (L5) with the backbone amide of Leu³³ and the Glu³⁴ carboxyl (L1), the main chain amide of Phe⁹³ (L3) with the Ser²⁰⁴ hydroxyl (L6), and Glu¹⁷⁶ carboxyl (L5a) with Ser⁹¹ hydroxyl (L3).
20. Superposition of the individual D1 and D2 domains of the native and EBP-EMP1 structures gives rmsd's of

- 0.92 Å (90 pairs) and 1.2 Å (98 pairs), respectively, for the C α atoms.
21. S. Atwell, M. Ultsch, A. M. de Vos, J. A. Wells, *Science* **278**, 1125 (1997); T. Clackson, M. H. Ultsch, J. A. Wells, A. M. de Vos, *J. Mol. Biol.* **277**, 1111 (1998); M. Huang *et al.*, *ibid.* **275**, 873 (1998).
22. L3 undergoes the largest change such that the relative position of Phe⁹³ is shifted 3.0 Å and 4.3 Å for its C α and phenyl ring, respectively. L6 undergoes shifts of 1.1 Å and 0.9 Å for the C α and phenyl ring, respectively, but the position of Phe²⁰⁵ remains relatively unperturbed.
23. F. P. Barbone *et al.*, *J. Biol. Chem.* **272**, 4985 (1997); L. K. Jolliffe *et al.*, *Nephrol. Dial. Transplant.* **10**, 28 (1985); S. A. Middleton *et al.*, *J. Biol. Chem.* **271**, 14045 (1996); S. A. Middleton *et al.*, in preparation.
24. K. Sawada, S. B. Krantz, S. T. Sawyer, C. I. Civin, *J. Cell. Physiol.* **137**, 337 (1988); K. Sawada *et al.*, *J. Clin. Invest.* **80**, 357 (1987); V. C. Broudy, N. Lin, M. Brice, B. Nakamoto, T. Papayannopoulou, *Blood* **77**, 2583 (1991).
25. N. L. Thompson *et al.*, *Photochem. Photobiol.* **65**, 39 (1997).
26. D. Langosch *et al.*, *J. Mol. Biol.* **263**, 525 (1996); B. Brosig and D. Langosch, *Protein Sci.* **7**, 1052 (1998); R. Laage and D. Langosch, *Eur. J. Biochem.* **249**, 540 (1997).
27. I. Remy, I. A. Wilson, S. W. Michnick, *Science* **283**, 990 (1999).
28. J. H. Naismith, T. Q. Devine, B. J. Brandhuber, S. R. Sprang, *J. Biol. Chem.* **270**, 13303 (1995); J. H. Naismith, T. Q. Devine, T. Kohno, S. R. Sprang, *Structure* **4**, 1251 (1996); J. H. Naismith, B. J. Brandhuber, T. Q. Devine, S. R. Sprang, *J. Mol. Recognit.* **9**, 113 (1996). These studies propose a related model for tumor necrosis factor receptor 1 (TNF-R1) in which the unliganded extracellular domains of the receptor may exist as a dimer on the membrane surface, and their cytoplasmic domains would then be separated by more than 100 Å. It has been unclear if this configuration exists in vivo because crystal structures of the TNF-soluble TNF receptor [D. W. Banner *et al.*, *Cell* **73**, 431 (1993)] have shown that the stoichiometry of the ligand bound receptor is 3:3. However, in light of our EPOR studies, the

- TNF-R1 unliganded structure may indeed be biologically relevant.
29. The interaction of an antibody with both its protein antigen and idiotypic antibody [B. A. Fields, F. A. Goldbaum, X. Yern, R. J. Polijak, R. A. Mariuzza, *Nature* **374**, 739 (1995)] and the plasticity of the T cell receptor recognition of foreign and self MHC-peptide antigens [K. C. Garcia *et al.*, *Science* **279**, 1166 (1998)] are further examples.
30. Crystallographic programs and methods. DENZO and SCALEPACK: Z. Otwinowski and W. Minor, *Methods Enzymol.* **276**, 307 (1997); AMoRE: J. Navaza, *Acta Crystallogr.* **A50**, 157 (1994); CCP4: S. Bailey, *ibid.*, p. 760; X-PLOR: A. T. Brünger, *ibid.* **A47**, 195 (1991); A. T. Brünger, *X-PLOR, Version 3.1: A system for x-ray and NMR* (Yale Univ. Press, New Haven, CT 1992); bulk solvent: J. S. Jiang and A. T. Brünger, *J. Mol. Biol.* **243**, 100 (1994); Program O: T. A. Jones, J. Y. Zou, S. W. Cowan, M. Kjeldgaard, *Acta Crystallogr.* **A47**, 110 (1991); PROCHECK: R. A. Laskowski, M. W. MacArthur, D. S. Moss, J. M. Thornton, *J. Appl. Crystallogr.* **26**, 283 (1993); GRASP: A. Nicholls, R. Bharadwaj, B. Honig, *Biophys. J.* **64**, 166 (1993).
31. $R_{\text{cryst}} = \frac{\sum |F_o| - |F_c|}{\sum F_o}$, where F_o and F_c are the observed and calculated structure factors, respectively. For $(I/\sigma(I))$, I is the measured intensity. For R_{free} the sum is extended over λ a subset of reflections (10%) excluded from all stages of refinement (1456 reflections). $R_{\text{sym}} = \frac{\sum \sum |I_i - \langle I \rangle|}{\sum I_i}$, where $\langle I \rangle$ is the average of equivalent reflections and the sum is extended over all measured observations for all unique reflections.
32. We thank J. Gately Luz for preparation of schematics in Fig. 1, K. Hotta for help with figures, S. Michnick and J. Kelly for helpful discussions, and R. Syed and R. Stroud for providing data for Fig. 2C. Supported in part by NIH grant GM49497 (I.A.W.) and the Ruff-Wormser Scholarship Fund (O.L.). This is publication 11901-MB from The Scripps Research Institute. The unliganded EBP coordinates have been deposited in the Protein Data Bank (PDB) with the accession code 1ern.

16 September 1998; accepted 12 January 1999

Erythropoietin Receptor Activation by a Ligand-Induced Conformation Change

Ingrid Remy,¹ Ian A. Wilson,² Stephen W. Michnick^{1*}

Erythropoietin and other cytokine receptors are thought to be activated through hormone-induced dimerization and autophosphorylation of JAK kinases associated with the receptor intracellular domains. An in vivo protein fragment complementation assay was used to obtain evidence for an alternative mechanism in which unliganded erythropoietin receptor dimers exist in a conformation that prevents activation of JAK2 but then undergo a ligand-induced conformation change that allows JAK2 to be activated. These results are consistent with crystallographic evidence of distinct dimeric configurations for unliganded and ligand-bound forms of the erythropoietin receptor.

The erythropoietin receptor (EpoR) shares both structural and functional features with the cytokine receptor superfamily that in-

cludes the interleukins, human growth hormone (hGH), and colony-stimulating factor (1, 2). Crystal structures and biochemical analysis have led to the generally accepted dimerization model of growth factor-mediated receptor activation, where monomeric receptors remain inactive until ligand binds to and oligomerizes the receptors, allowing autophosphorylation of receptor-associated intracellular kinases (3). However, dimerization or oligomerization of receptors is a

¹Département de Biochimie, Université de Montréal, Casier Postal 6128, succursale Centre-ville, Montréal, Québec, H3C 3J7, Canada. ²Department of Molecular Biology and the Skaggs Institute for Chemical Biology, The Scripps Research Institute, 10550 North Torrey Pines Road, La Jolla, CA 92037, USA.

*To whom correspondence should be addressed.

REPORTS

required but not necessarily sufficient condition for receptor activation.

Studies of hGH bound to human growth hormone receptor (hGHR) and of Epo, agonist, or antagonist peptides bound to EpoR have shown that all of these ligands bind to receptor dimers with different dimer interface orientations, which correlate with differences in the efficiency of receptor activation (4). Livnah *et al.* have also determined the crystal structure of unliganded EpoR and show that it is also a dimer, but with a dramatically different arrangement of the two subunits (5). A significant feature of the unliganded extracellular dimer is that the COOH-termini of the monomers, the points of insertion into the membrane, are separated by 73 Å, compared with 39 Å when the agonist peptide EMP1 is bound to EpoR. On the basis of this finding and the ligand-bound structures, they propose an alternative allosteric mechanism of receptor activation in which ligand-induced re-

organization of the dimer brings the intracellular domains into closer proximity, allowing associated JAK2s to come into contact and autophosphorylate (Fig. 1A).

To test this model, we used a fluorescent assay based on dimerization-induced complementation of designed fragments of the murine enzyme dihydrofolate reductase (DHFR) (6, 7). The basis for the assay is that complementary fragments of DHFR, when they are fused to interacting proteins and expressed in cells, will reassemble and bind to the high-affinity (dissociation constant $K_d = 540$ pM) fluorescein-conjugated inhibitor methotrexate (fMTX) in a 1:1 complex. The fMTX is retained in cells by this complex, whereas unbound fMTX is actively transported out of the cells (8). fMTX-DHFR complexes can be monitored by fluorescence microscopy, fluorescence-activated cell sorting (FACS), or spectroscopy. To test the allosteric model we reasoned as follows: if the receptor dimer transmembrane domains are separated by the

distance observed in the crystal structure of unliganded EpoR (73 Å), then DHFR fragments (F[1,2] and F[3]) fused to the COOH-termini of the transmembrane domains will complement only if ligand induces the conformation change that allows the fragments to fold into the precise three-dimensional structure of DHFR (Fig. 1B) (7, 9). This requires that the NH₂-termini of the DHFR fragments be 8 Å apart. Insertion of flexible linker peptides between the transmembrane domain and DHFR fragments allowed us to probe the distance between the insertion points of the extracellular domain dimer. Linkers of 5, 10, and 30 amino acids allowed us to probe the range of possibilities as they correspond to extended lengths of 20, 40, and 120 Å, respectively (~4 Å per peptide bond). It would be predicted that with 5-amino acid (5-aa) linkers, complementation of the DHFR fragments would only occur in the presence of ligands (Fig. 1B), with 10-amino acid (10-aa) linkers some complementation could occur in the absence of ligand, but with

Fig. 1. Schematic representation of the crystallographic structure-based Epo receptor activation hypothesis and of the experimental strategy. (A) Receptors are dimers in their unliganded state (5). The extracellular domain exists in a conformation that holds the intracellular domains and associated JAK2s separated from each other by ~73 Å. On binding ligand (Epo or peptide agonist EMP1), the extracellular dimer is reorganized, bringing the intracellular domains to within 39 Å of each other, allowing autophosphorylation and activation of the JAK2s. (B and C) The extracellular and transmembrane domains of murine EpoR [EpoR(1-270)] are fused to one of two complementary fragments of murine DHFR (F[1,2] or F[3]) through flexible linkers (gray lines) consisting of (Gly-Gly-Gly-Gly-Ser)_N repeats where N = 1, 2, or 6 to generate the following: EpoR(1-270)-5aa-F[1,2] or -F[3], EpoR(1-270)-10aa-F[1,2] or -F[3], and EpoR(1-270)-30aa-F[1,2] or -F[3]. Cells transfected with these fusions express receptors at the membrane surface. Fluorescein-methotrexate (fMTX) is taken up by cells and binds to reconstituted DHFR (F[1,2]+F[3]) and is retained in the cell. Unbound fMTX is rapidly released from the cells by active transport (8). Panel (B) shows how fusions in which DHFR fragments are connected to receptors by a 5-aa linker cannot complement in the unliganded receptor. When receptors bind to Epo or EMP1, DHFR fragment complementation can take place. In panel (C), fusions with the 30-aa linker allow complementation of DHFR fragments whether receptors are ligand-bound or not. (D) Results of complementation experiments with EpoR extracellular and transmembrane domains should be reproducible with complete EpoR receptor complex, including associated JAK2. Here is shown one such experiment in which DHFR fragments are fused to the COOH-terminal of JAK2 and co-expressed in cells along with full-length EpoR.

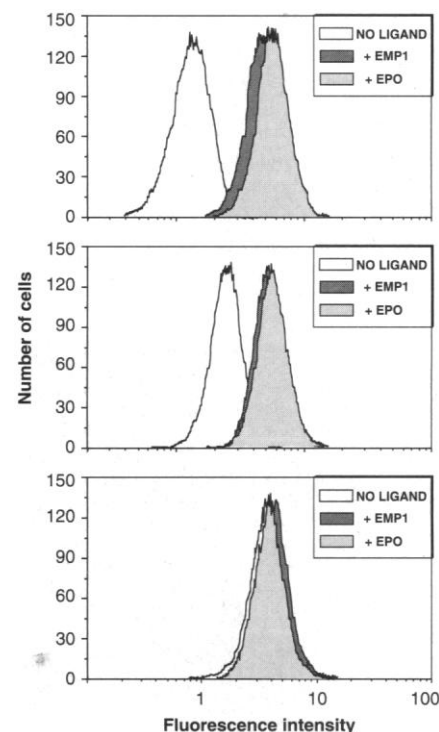
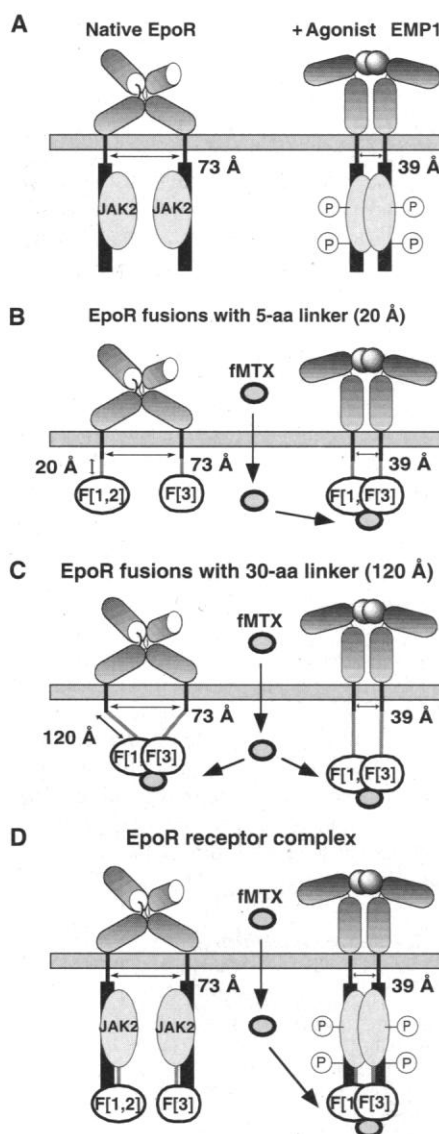


Fig. 2. Fluorescence flow cytometric analysis of CHO DUKX-B11 cells labeled with fMTX. Cells were transfected with EpoR(1-270)-5aa-F[1,2] and -F[3] (top), with EpoR(1-270)-10aa-F[1,2] and -F[3] (middle), and with EpoR(1-270)-30aa-F[1,2] and -F[3] (bottom). Histograms are based on analysis of fluorescence intensity for 10,000 cells at flow rates of ~1000 cells per second. Data were collected on a Coulter XL 4 color FACS analyzer (Coulter-Beckman) with stimulation by an argon laser tuned to 488 nm with emission recorded through a 525-nm band width filter. Histograms represent the response in absence of ligands (white histogram), with 10 nM Epo (light gray histogram), or with 10 μM EMP1 (dark gray histogram). Constructs and methods are described in (16).

REPORTS

30-amino acid (30-aa) linkers it would be independent of ligand (Fig. 1C).

CHO DUKX-B11 (DHFR⁻) cells were cotransfected with EpoR extracellular and transmembrane domains [EpoR(1-270)] fused to peptide linkers and one of the two DHFR fragments F[1,2] or F[3]. Cotransfectants were selected for survival in the presence of Epo (2 nM), to induce DHFR complementation, in nucleotide-free medium (selection for DHFR activity). Fluorescence flow cytometric analysis of the cotransfectants incubated with fMTX showed significant increases (by a factor of ~8) in fluorescence over background levels when cells were treated with Epo or EMP1. In the absence of ligands, cells transfected with EpoR-DHFR fragment fused through 5-aa linkers showed no fluorescence, compared with non-transfected cells; cells with a 10-aa linker showed a weak fluorescence, whereas those expressing fusions with a 30-aa linker showed the same level of fluorescence in the presence or absence of ligands (Fig. 2). These results are consistent with the allosteric model of Livnah *et al.* (5) and cannot be due to steric hindrance caused by proteins at the membrane intracellular surface that might prevent DHFR fragment complementation for the shorter 5-aa and 10-aa linkers. If this was the case, the signal seen in the presence of ligand for the 30-aa linker, and to some extent for the 10-aa linker, would be higher than for the 5-aa linker. In fact, the fluorescence intensity and number of activated receptors as determined spectroscopically

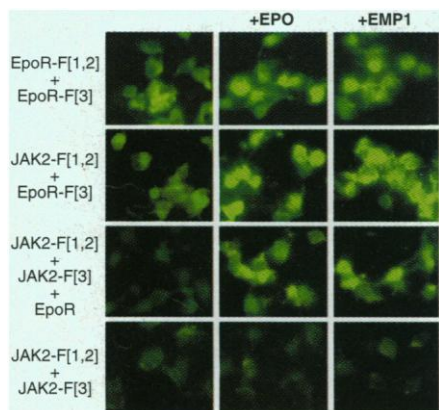


Fig. 3. Fluorescence microscopy of COS-7 cells expressing EpoR-DHFR and JAK2-DHFR fragment fusions. Cells were grown on 18-mm glass coverslips to $\sim 3 \times 10^5$ in Dulbecco's modified Eagle's medium (Life Technologies) enriched with 10% cosmic calf serum (Hyclone) in 12-well plates. Plasmids pMT3 harboring full-length EpoR or EpoR and JAK2 fused through a 5-aa linker to F[1,2] or F[3] were created and cells were transiently transfected with the different constructs. Cells were prepared as described in (16) for FACS except that after the last wash with PBS, cells were mounted on glass slides. Fluorescence microscopy was performed on live cells with a Zeiss Axiophot microscope (objective lens Zeiss Plan Neofluar 40 \times /0.75).

(about 8500 receptors per cell) is the same in all three cases (10). Furthermore, dose-response analyses based on FACS data showed saturable single-site binding with K_d 's of 164 pM and 168 nM for Epo and EMP1, respectively (10). These results are consistent with previous binding studies (1, 11).

To demonstrate that the allosteric model applies to the complete receptor complex, we coexpressed full-length EpoR and JAK2 in COS-7 cells fused to complementary F[1,2] and F[3] fragments through the 5-aa linker (Fig. 3). Coexpression of EpoR-F[1,2] with EpoR-F[3] gave a response in the absence of ligands. These results are consistent with circular dichroism and nuclear magnetic resonance studies showing that the intracellular domain of EpoR is partially unfolded in the absence of JAK2 (12). Taken with our results presented here, we suggest that the 236-amino acid intracellular domain acts as a very long linker itself, resulting in reconstitution of DHFR. Fluorescence was also seen when JAK2-F[1,2] was coexpressed with EpoR-F[3] in the absence of ligands, consistent with previous studies indicating that this interaction is constitutive (13). JAK2-F[1,2] and JAK2-F[3] coexpressed with full-length EpoR (not fused to either F[1,2] or F[3]; see Fig. 1D) showed an induced response to Epo or EMP1. This key result demonstrates that coupling of a ligand-induced conformational change in the extracellular domain allows two JAK2s associated with the receptor intracellular domain to come into proximity. Finally, coexpressed alone, JAK2-F[1,2] and JAK2-F[3] showed no detectable fluorescence. Cotransfected EpoR and JAK2 was also shown to function normally with the attached F[1,2] or F[3] fragments because ligand-induced phosphorylation of JAK2 and EpoR were detected (12).

The results presented here are consistent with the structural allosteric model of Livnah *et al.* (5) (Fig. 1A). The model is not contradictory to dimerization models; dimerization is a required, but not necessarily sufficient, condition for receptor activation. Fluorescence resonance energy transfer studies have demonstrated that other receptors may exist as preformed dimers, including those for interleukin-1, interleukin-2, and epidermal growth factor (14). Investigation with strategies such as those described here will help to determine if these and other receptors may be activated by a similar mechanism as that of EpoR.

References and Notes

1. A. D. D'Andrea, G. D. Fasman, H. F. Lodish, *Cell* **58**, 1023 (1989).
2. J. F. Bazan, *Proc. Natl. Acad. Sci. U.S.A.* **87**, 6934 (1990); N. Stahl and G. D. Yancopoulos, *Cell* **74**, 587 (1993).
3. C. H. Heldin, *Cell* **80**, 213 (1995).
4. hGH-hGHR: A. M. De Vos, M. Ultsch, A. A. Kossiakoff, *Science* **255**, 306 (1992); Epo-EpoR: R. S. Syed *et al.*, *Nature* **395**, 511 (1998); EMB1-EpoR: O. Livnah *et al.*,

Science **273**, 464 (1996); EMP33-EpoR: O. Livnah, *et al.*, *Nature Struct. Biol.* **5**, 993 (1998).

5. O. Livnah *et al.*, *Science* **283**, 987 (1999).
6. J. N. Pelletier and S. W. Michnick, *Protein Eng.* **10**, 89 (1997).
7. J. N. Pelletier, F. Campbell-Valois, S. W. Michnick, *Proc. Natl. Acad. Sci. U.S.A.* **95**, 12141 (1998).
8. R. J. Kaufman, J. R. Bertino, R. T. Schimke, *J. Biol. Chem.* **253**, 5852 (1978); D. I. Israel and R. J. Kaufman, *Proc. Natl. Acad. Sci. U.S.A.* **90**, 4290 (1993).
9. V. Cody, J. R. Luft, E. Ciszak, T. I. Kalman, J. H. Freisheim, *Anti-Cancer Drug Des.* **7**, 483 (1992).
10. CHO DUKX-B11 cells expressing the different fusions were grown to confluence and treated with fMTX as described in (16). After a phosphate-buffered saline (PBS) wash, cells were lysed with detergent and centrifuged (20,000g for 10 min) to remove debris and unlysed cells. The supernatant was heated to 95°C for 10 min and centrifuged again to remove protein precipitate. Extracted fMTX was analyzed on a Luminescence Spectrometer (Perkin-Elmer LS50B) (excitation and emission wavelengths: 497 nm \pm 5 nm and 516 nm \pm 5 nm). The concentration of fMTX in each sample was determined by direct comparison to a standard curve of fluorescence intensity versus fMTX concentration. The number of receptors per cell was calculated according to the following equation:

$$\frac{\text{nb EpoR}}{2} = \frac{[\text{fMTX}]_s \times V_s \times \text{Av. nb}}{(\text{nb cells})_s}$$

where nb EpoR is the number of receptors, [fMTX]_s is the concentration of fMTX determined in the sample, V_s is the volume of the sample, Av. nb is Avogadro's number (6.022×10^{23} molecules per mole), and (nb cells)_s is the number of cells in the sample. Dose-response studies were performed for Epo and EMP1 based on flow cytometric analysis of CHO DUKX-B11 cells expressing EpoR(1-270)-5aa-F[1,2] and -F[3]. Mean fluorescence intensities were determined for three separate samples at each ligand concentration (between 0.0003 nM and 100 nM for Epo, or between 0.0003 μ M and 100 μ M for EMP1). Data points were fit with a nonlinear least squares algorithm to a Langmuir isotherm determined in the computer program MacCurveFit (Kevin Raner Software) with a Quasi-Newton optimization routine (the correlation coefficient r^2 and residual error for the Epo curve were 0.98 and 0.045, respectively, and for the EMP1 curve, 0.99 and 0.022, respectively).

11. A. D. D'Andrea *et al.*, *Mol. Cell Biol.* **11**, 1980 (1991); D. L. Johnson *et al.*, *Biochemistry* **37**, 3699 (1998); N. C. Wrighton *et al.*, *Science* **273**, 458 (1996); N. C. Wrighton *et al.*, *Nature Biotechnol.* **15**, 1261 (1997).
12. I. Remy and S. W. Michnick, data not shown.
13. B. A. Witthuhn *et al.*, *Cell* **74**, 227 (1993).
14. C. Guo, S. K. Dower, D. Holowka, B. Baird, *J. Biol. Chem.* **270**, 27562 (1995); S. Damjanovich *et al.*, *Proc. Natl. Acad. Sci. U.S.A.* **94**, 13134 (1997); T. Gadella Jr. and T. M. Jovin, *J. Cell Biol.* **129**, 1543 (1995).
15. R. J. Kaufman, *Proc. Natl. Acad. Sci. U.S.A.* **82**, 689 (1985).
16. All fusion clones were generated by polymerase chain reaction amplification of the individual genes of interest. The construction of the DHFR F[1,2] and F[3] are described in (7). Oligonucleotides coding for flexible linker peptides were synthesized individually with 5' and 3' complementary overhangs corresponding to 5' or 3' insertion between EpoR- and DHFR fragment-encoding sequences. Regions of each construct were subcloned into the mammalian expression vector pMT3 (15). Lipofectamine (Life Technologies) was used to stably transfect cells with EpoR-DHFR fragments, and stable colonies were selected on minimum essential medium (Life Technologies) enriched with 10% dialyzed fetal bovine serum (FBS) (Hyclone) (dialyzed to remove nucleotides, rendering cells dependent on exogenous DHFR activity) and in the presence of 2 nM human recombinant Epo (R. W. Johnson Pharmaceutical Research Institute). fMTX (Molecular Probes) was added to each sample at a final concentration of 10 μ M and incubated for 22 hours at 37°C without Epo. Cells were then treated with 10 nM Epo or 10 μ M EMP1 (RW) for 30 min at 37°C. The medium was removed and the cells were

washed with PBS and incubated again for 30 min in α -MEM with Epo or EMP1 to allow for efflux of unbound fMTX. Medium was removed and cells were washed with PBS, treated with trypsin, and suspended in 500 μ l of cold PBS supplemented with 10% FBS to increase cell viability and kept on ice before cytometric analysis within 20 min.

17. We gratefully acknowledge gifts of pMT3 vector and CHO DUKX-B11 cell line and helpful advice from M.

Davies (Genetics Institute), EpoR and JAK2 clones from U. Klingmüller (Max Planck Institute for Immunobiology, Freiburg), and EMP1, Epo, and helpful discussion from D. Johnson and L. Jolliffe (R. W. Johnson Pharmaceutical Research Institute), and we thank M. Powell for timely advice. Supported by the Burroughs Wellcome Fund (S.W.M.) and NIH grant GM49497 (I.A.W.).

15 September 1998; accepted 12 January 1999

Hunting Behavior of a Marine Mammal Beneath the Antarctic Fast Ice

R. W. Davis,¹ * L. A. Fuiman,² T. M. Williams,³ S. O. Collier,¹ W. P. Hagey,⁴ S. B. Kanatous,⁵ S. Kohin,⁵ M. Horning¹

The hunting behavior of a marine mammal was studied beneath the Antarctic fast ice with an animal-borne video system and data recorder. Weddell seals stalked large Antarctic cod and the smaller subice fish *Pagothenia borchgrevinki*, often with the under-ice surface for backlighting, which implies that vision is important for hunting. They approached to within centimeters of cod without startling the fish. Seals flushed *P. borchgrevinki* by blowing air into subice crevices or pursued them into the platelet ice. These observations highlight the broad range of insights that are possible with simultaneous recordings of video, audio, three-dimensional dive paths, and locomotor effort.

The process by which mammalian predators search for, locate, stalk, and subdue their prey has been the subject of considerable research efforts for terrestrial species (1). In contrast, less is known about the foraging behavior of marine mammals, primarily because they are so difficult to observe underwater. Direct observation of marine animal behavior with scuba, fixed-location cameras, remotely operated vehicles, and manned submersibles is limited by depth or duration. Often these technologies provide only fleeting glimpses of highly mobile species. Animal-borne time-depth recorders and acoustic tracking provide information on diving performance (2, 3) but do not allow direct observation of animals at depth. As a result, our knowledge of the underwater behavior of marine mammals, especially deep diving species, is based primarily on indirect information provided by dive depth and duration statistics and estimated swim speeds. To provide a better understanding of marine mammal diving and hunting behavior, we developed an animal-borne vid

eo system and data recorder that enabled us to observe Weddell seals (*Leptonychotes weddellii*) foraging at depth and to compute their three-dimensional dive paths.

Weddell seals are large, marine predators that are highly adapted for hunting in shore-fast and pack ice habitats (2, 4). To forage beneath the extensive, unbroken fast ice, these seals must locate, pursue, and capture prey in three spatial dimensions under low-light conditions and while holding their breath. Foraging is thought to occur in daily bouts consisting of up to 40 consecutive dives. These dives are usually to depths of 100 to 350 m (the maximum recorded dive depth is 741 m) and less than 25 min long. Analyses of partially digested prey, fish otoliths, and skeletal material obtained from stomach samples and feces indicate that Weddell seals consume a variety of prey, although local diets appear narrow (2, 5). For example, Weddell seals in McMurdo Sound, Antarctica, forage primarily on small nototheniid fish (*Pleuragramma antarcticum*, *Pagothenia borchgrevinki*, and *Trematomus* spp.). They also capture large Antarctic cod, which grow to 165 cm in length and weigh up to 77 kg (5). However, virtually nothing is known about how Weddell seals find their prey, where they find it, and how they stalk and capture it.

We attached a small video system and data logger (6) to four adult Weddell seals (one male and three females) from October to December 1997 to study their hunting behavior in the fast ice environment of McMurdo Sound, Antarctica. The video system recorded images of the seal's head and the environment immediately in

front of the animal. The data logger recorded time, depth, water speed, and compass bearing once per second, and flipper stroke frequency and ambient sound were recorded continuously on the audio channels. These data enabled us to compute the seals' three-dimensional dive paths and locomotor effort.

In 57.4 hours of underwater video and data recordings, we observed several encounters between seals and their known prey. Three of these encounters were midwater interactions with Antarctic cod. One dive by seal 4, a 462-kg female, provides details on how Weddell seals stalk large prey in three dimensions. This seal departed the breathing hole and descended at an average swim speed of 1.3 m s⁻¹ to a depth of 51 m (Fig. 1A). Without changing horizontal direction (bearing), the seal then ascended to 33 m at 1.2 m s⁻¹ and began a second, gliding descent at 0.7 m s⁻¹. We surmise that the seal visually located a cod and began to stalk it at 4 min 51 s into the dive and a depth of 53 m when the seal suddenly accelerated to speeds of almost 2 m s⁻¹ with large swimming strokes. At this point, the seal was about 23 m from the cod. Before this (minute 4 of the dive), the seal had been gliding at a descent angle of 31° along a straight course, bearing 103°, which almost intersected the point of contact with the cod (Fig. 1, A and B). Instead of continuing directly toward the fish, the seal leveled its descent and veered 28° to the right with the sudden acceleration (Fig. 1, A and B). This bearing took the prey out of the seal's line of sight and increased the distance between them. At 5 min 39 s into the dive and a distance of 28 m from the cod, the seal accelerated through a looping turn and a 23° descent to 73 m, reaching speeds in excess of 2 m s⁻¹ and bringing it beneath a very large (>1 m long) Antarctic cod (Fig. 1C). The seal extended its neck and struck the cod near the anal fin with its muzzle. The fish reacted vigorously with a powerful tail thrust and disappeared from view; it was not seen again. By attacking from below at the posterior part of the fish, the seal silhouetted the cod against the under-ice surface and remained out of sight. The seal did not appear to pursue the cod after the strike but continued descending to 85 m. At the bottom of the dive, the seal turned left and then ascended quickly to the ice hole at an average speed of 1.8 m s⁻¹.

Two other encounters with Antarctic cod were recorded: one by a 475-kg male (seal 2) and another by seal 4. The seals approached to within centimeters of the fish, from slightly below or horizontally, without eliciting a response. The cod encountered by seal 2 was at a depth of less than 20 m and strongly backlit by the under-ice surface. As the seal approached, it extended its head with erect vibrissae toward the fish. The seal vocalized briefly as it swam over the fish. Seal 4 approached a cod against a dark background at a

¹Department of Marine Biology, Texas A&M University, 5007 Avenue U, Galveston, TX 77553, USA.

²Department of Marine Science, University of Texas at Austin, 750 Channel View Drive, Port Aransas, TX 78373, USA. ³Department of Biology, EMS-A316, University of California, Santa Cruz, CA 95064, USA. ⁴Pisces Design, 7660 Fay Avenue, Suite H-186, La Jolla, CA 92037, USA. ⁵University of California School of Medicine, 0623A, 9500 Gillman Drive, La Jolla, CA 92093, USA.

*To whom correspondence should be addressed. E-mail: davisr@tamug.tamu.edu